Supplementary Information (SI) for Nanoscale.
This journal is © The Royal Society of Chemistry 2025

Electronic Supplementary Information

$Ni_2P/NiMoO_x$ Nanocone Electrocatalyst for Efficient Hydrogen Evolution: Tip-enhanced Local Electric Field Effect

Le Yu[1], Xia Chen[1], Shunda Cheng, Tingfeng Zhong, Ruifan Zhou, Zihua Deng * and Li Li

College of Chemistry and Chemical Engineering, Chongqing University, Chongqing, China.

1.The authors contributed equally.

* *Corresponding Author. E-mail: hg2531@cqu.edu.cn*

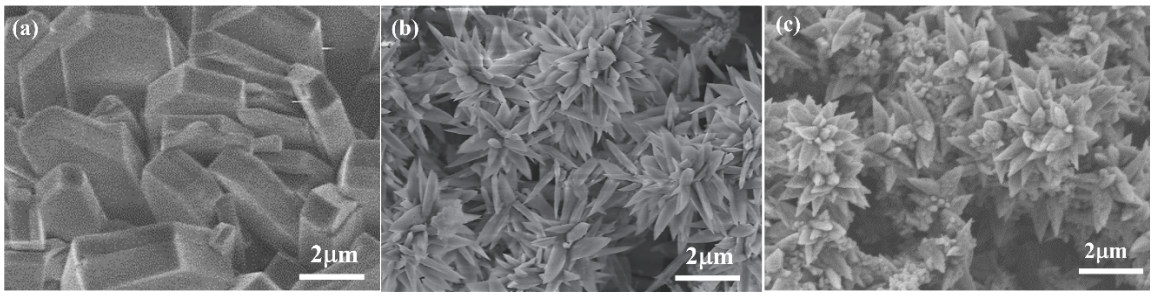

Fig. S1 SEM images of (a) Ni–BDC, (b) $NiMoO_x$, (c) $Ni_2P/NiMoO_x$ nanocones.

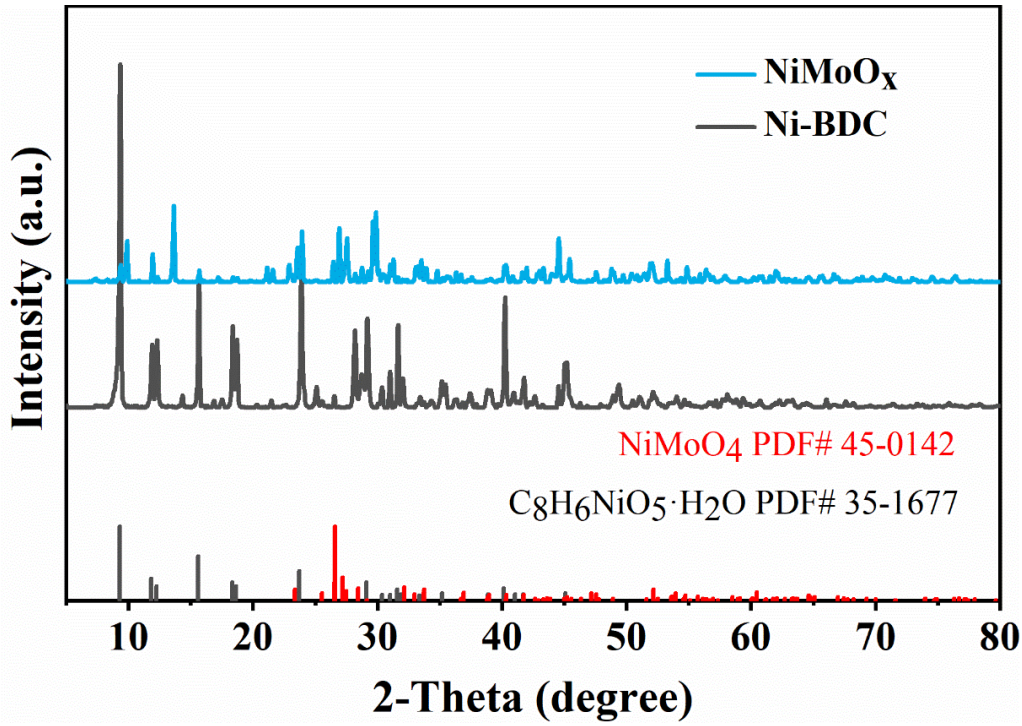

Fig. S2 XRD patterns of Ni–BDC and $NiMoO_x$.

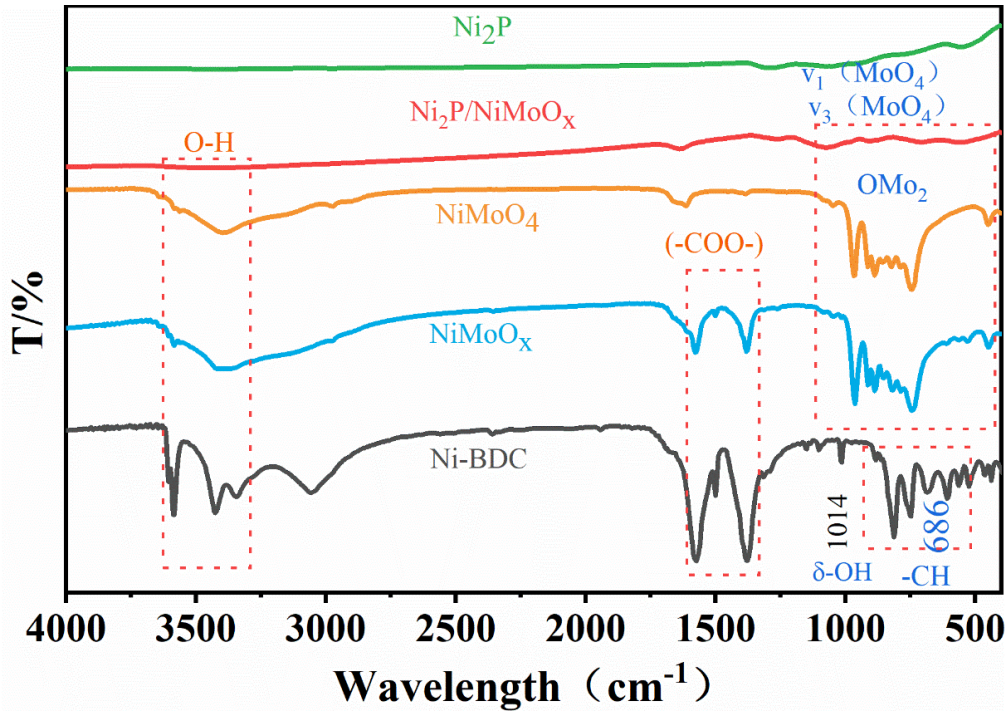

Fig. S3 FTIR patterns of Ni–BDC, $NiMoO_x$, $NiMoO_4$, Ni_2P and $Ni_2P/NiMoO_x$ nanocones.

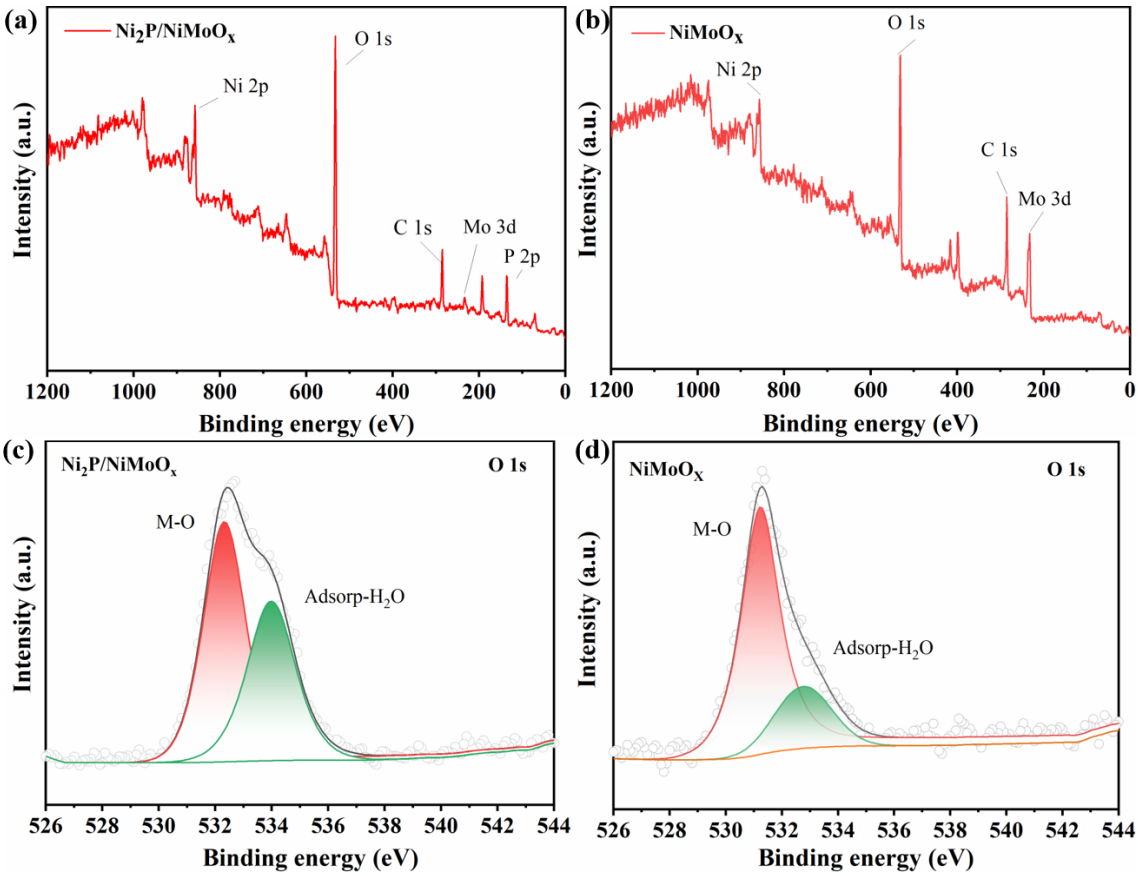

Fig. S4 XPS spectra of survey (a, b), O 1s (c, d) for $Ni_2P/NiMoO_x$ nanocones and $NiMoO_x$.

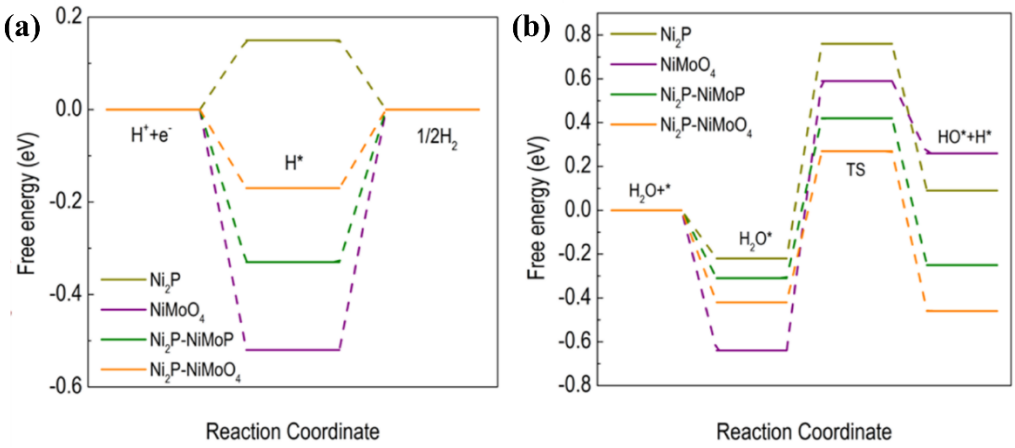

Fig. S5 (a) ΔG_{H^*} diagram of Ni_2P, $NiMoO_4$, Ni_2P-NiMoP, and Ni_2P-$NiMoO_4$[1],

(b) Reaction energy diagram of water dissociation on Ni_2P, $NiMoO_4$, Ni_2P-NiMoP, and Ni_2P-$NiMoO_4$ [1].

DFT for similar compositions of Ni_2P-$NiMoO_x$ has been reported in the literature[1]. Figure S5a shows that the ΔG_{H^*} value of the Ni_2P-$NiMoO_4$ heterostructures significantly decreases, indicating that the interactions of Ni_2P and $NiMoO_4$ have a satisfying effect on optimizing the adsorption of H* [1]. Figure S5b shows the corresponding reaction energy profile. The results show that the Ni_2P-$NiMoO_4$ heterostructures are more favorable for H_2O adsorption, accelerating the Volmer step and enhancing the activity of HER.[1]

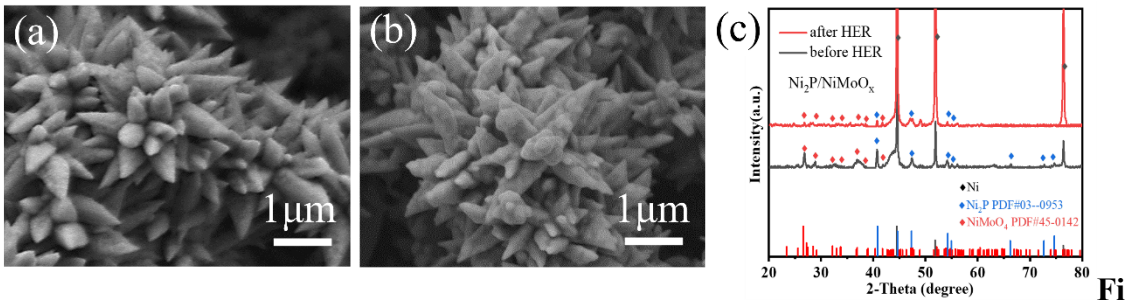

Fig. S6 $Ni_2P/NiMoO_x$ nanocones SEM image before (a) and after (b) 200 h durability test，and XRD pattern (c).

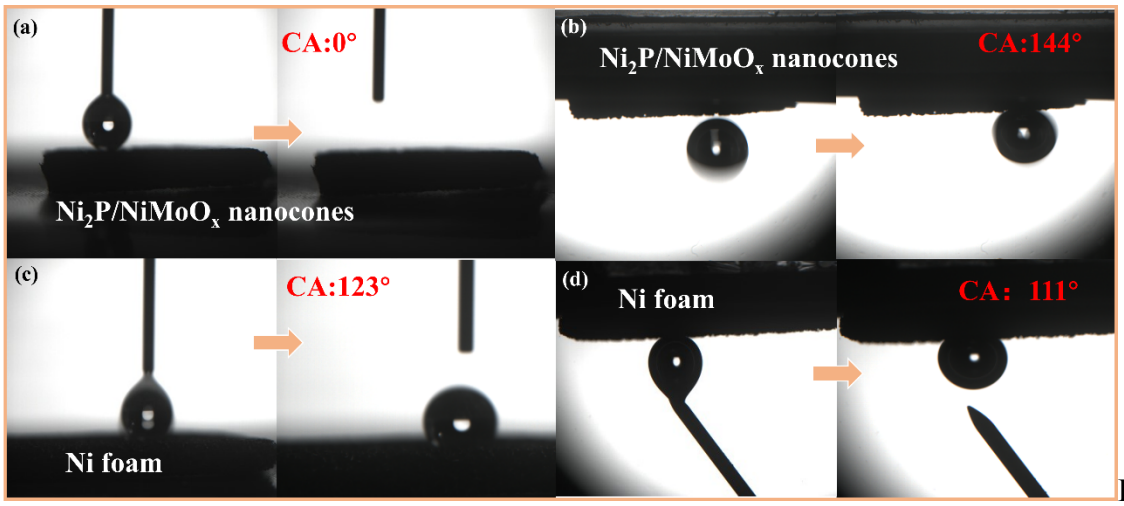

Fig. S7 Images of (a) droplet contact angles (CA) and (b) H_2–bubble CA on $Ni_2P/NiMoO_x$ nanocones, images of (c) droplet CA and (d) H_2-bubble CA on blank NF

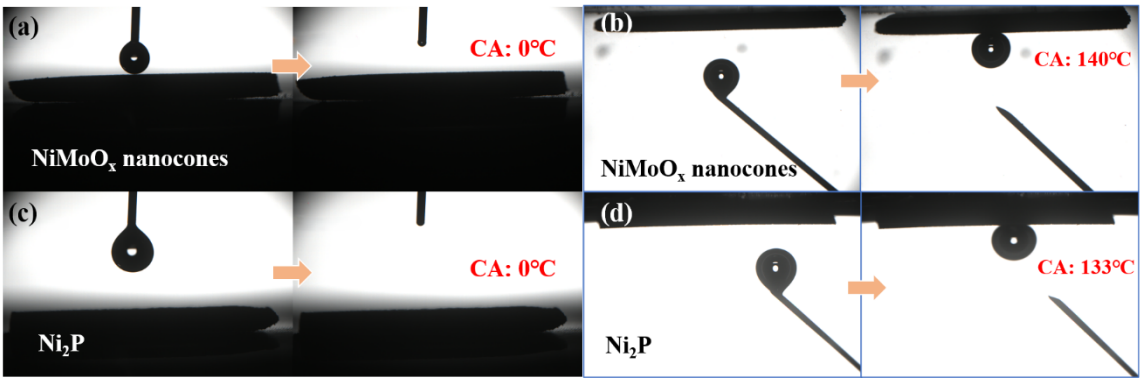

Fig. S8 Images of (a) droplet CA and (b) H_2-bubble CA on $NiMoO_x$ nanaoconesand, images of (c) droplet CA and (d) H_2-bubble CA on Ni_2P.

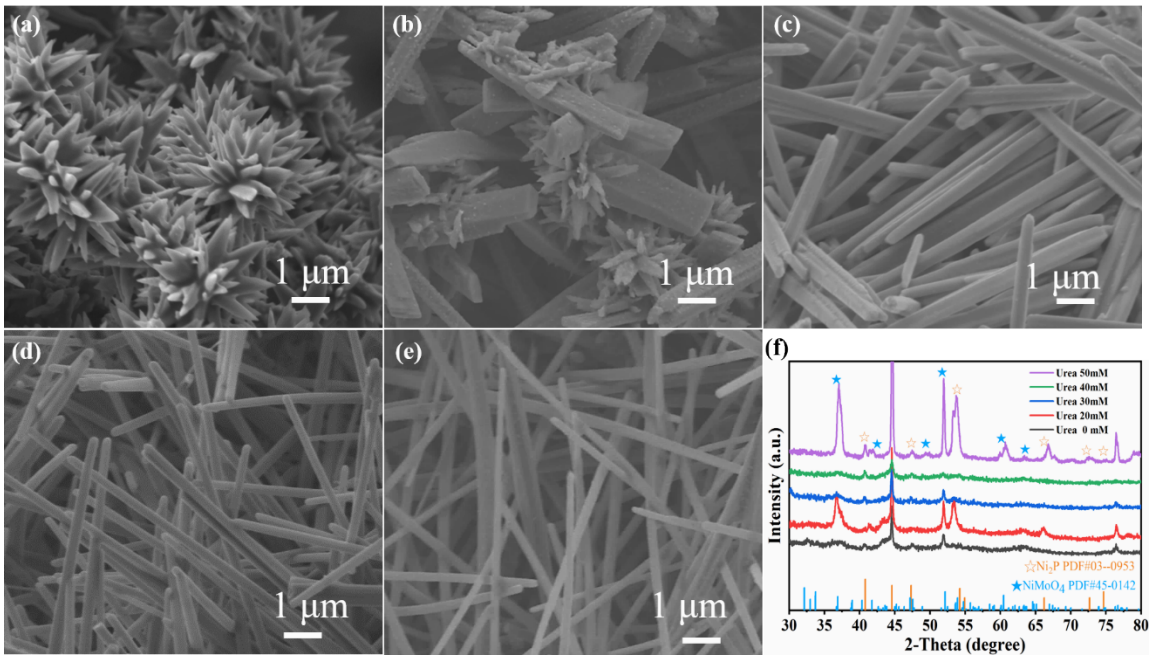

Fig. S9 SEM images of $Ni_2P/NiMoO_x$ prepared with different urea concentrations: (a) 0 mM urea; (b) 20 mM urea; (c) 30 mM urea; (d) 40 mM urea; (e) 50 mM urea; (f) XRD pattern of $Ni_2P/NiMoO_x$ samples.

$Ni_2P/NiMoO_x$ samples were synthesised using a method similar to that of $Ni_2P/NiMoO_x$ nanocones, except for the addition of urea during the second step of the synthesis. The different morphologies of the $Ni_2P/NiMoO_x$ samples (Fig. S9a – S9e) exhibited identical material compositions (Fig. S9f). And with the increase of urea concentration, the nanocone structures are gradually dissolved and converted into nanorods.

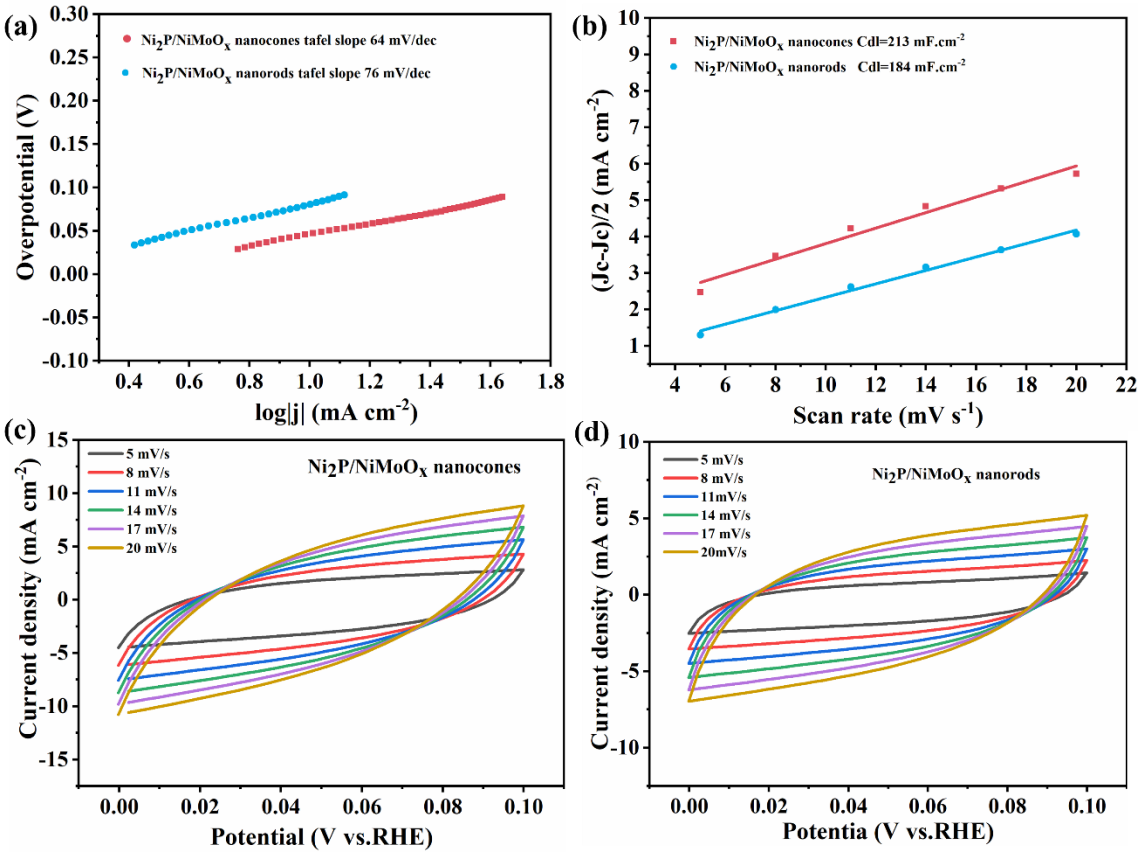

Fig. S10 (a) Tafel slopes，(b) Double layer capacitor，(c) CV curves of $Ni_2P/NiMoO_x$ nanocones and (d) $Ni_2P/NiMoO_x$ nanorods under different scan rates.

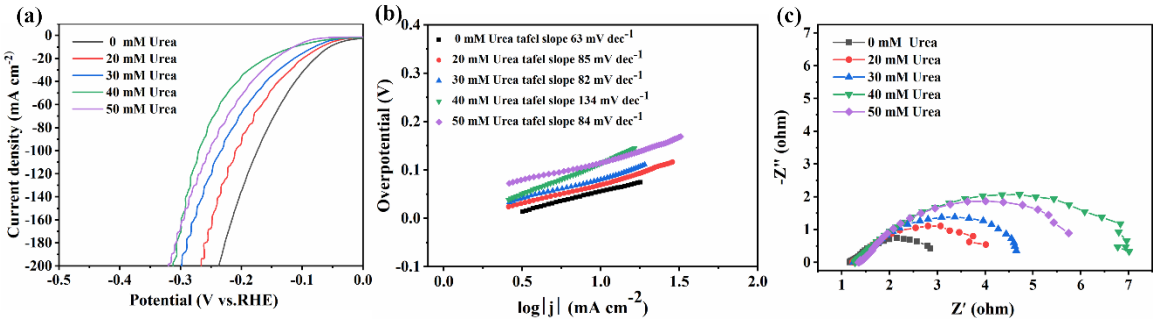

Fig. S11 (a) LSV curves, (b) Tafel slopes, (c) Nyquist plots of $Ni_2P/NiMoO_x$ sample by adding different concentrations of urea during the second step of the synthesis.

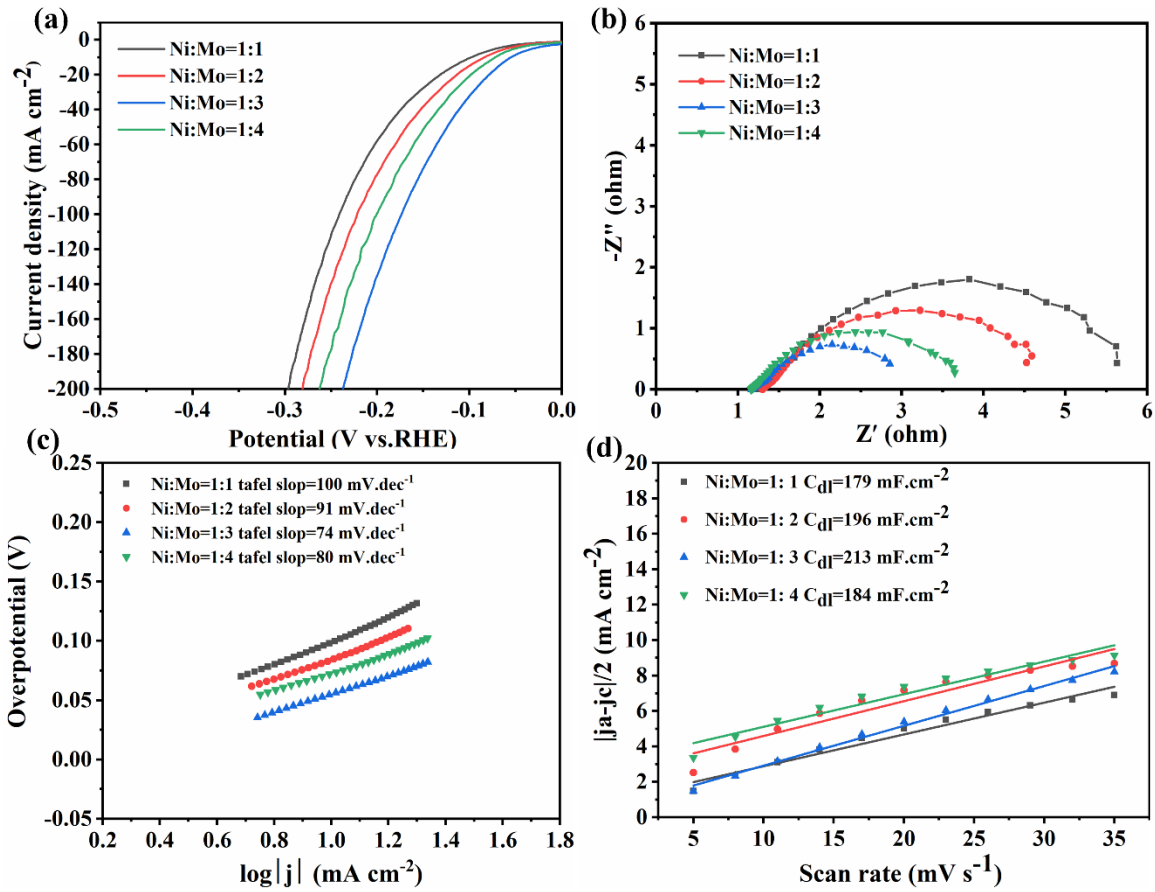

Fig. S12 (a) LSV curves, (b) Tafel slopes, (c) Nyquist plots and (d) Double layer capacitor of $Ni_2P/NiMoO_x$ with different Ni:Mo feeding ratios in 1 M KOH.

In order to prepare $Ni_2P/NiMoO_x$ nanocones catalyst with excellent performance and nanocone structure, the effect of ammonium molybdate feed ratio was investigated. With the increase of the atomic molar ratio of Ni:Mo, the morphology of $Ni_2P/NiMoO_x$ changes from nanosheet array to nanocone array. When Ni:Mo molar ratio of 1:3, the $Ni_2P/NiMoO_x$ nanocones showed the best electrochemical performance and uniform distribution of nanocone (Fig S12-S13).

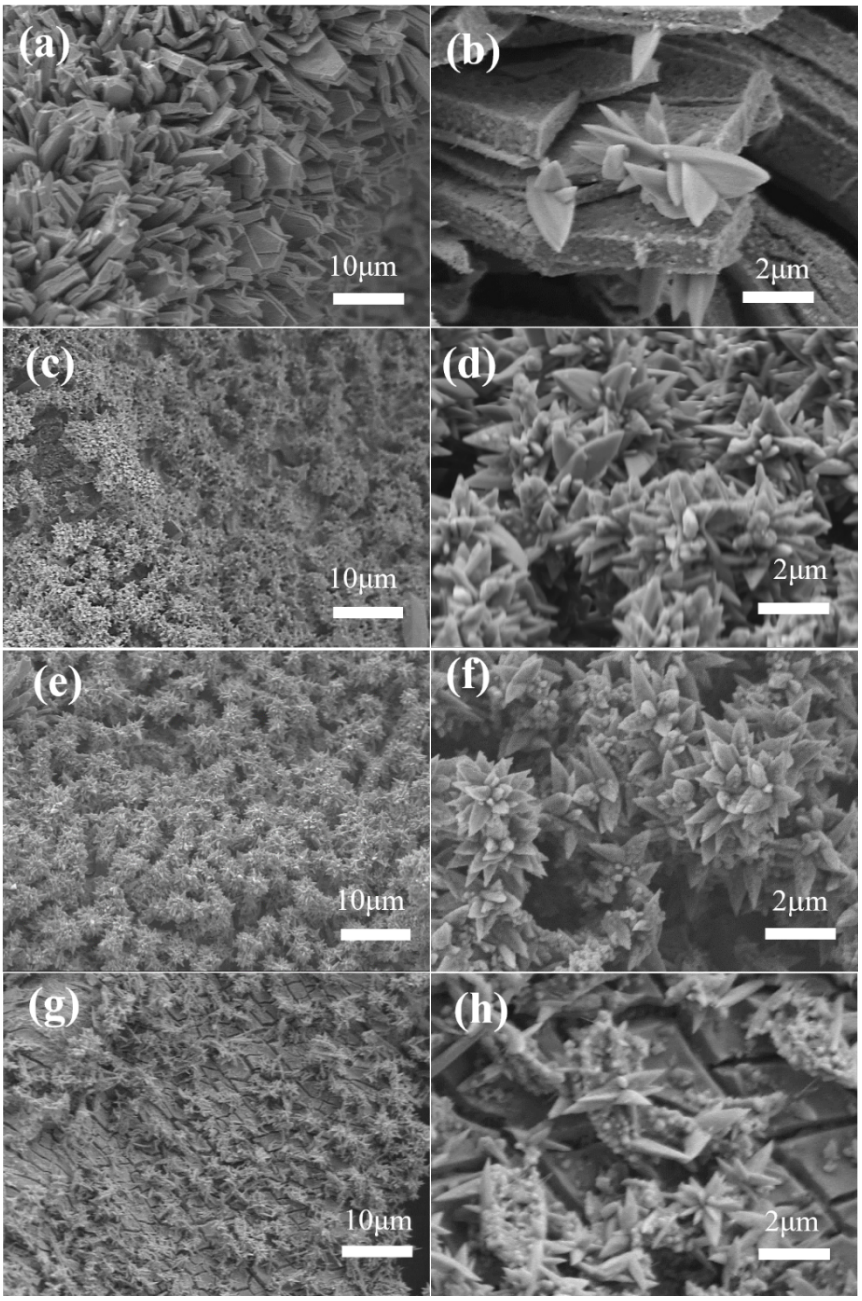

Fig. S13 SEM images of $Ni_2P/NiMoO_x$ (a-b）Ni:Mo=1:1, (c-d) Ni:Mo=1:2, (e-f）Ni:Mo=1:3, (g-h）Ni:Mo=1:4.

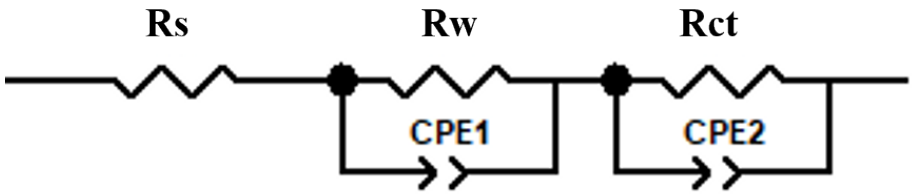

Fig. S14 Equivalent electrical circuit used to fit with the EIS data**.**

EIS is not get affected by potential drop due to series resistance, and could reveal the intrinsic electrochemical properties of the catalyst interface. The Nyquist plots were fitted using the equivalent electric circuit (EEC) presented in Fig. S14. This EEC corresponds to a simple heterogeneous adsorption step. In this context, R represents the resistance component, and constant phase element (CPE) represents the capacitive component, which is used in cases of modified electrodes and electrodes coated with nanostructured materials with a high roughness factor. Rs is related to the solution impedance, R_w and CPE1 are associated with solution diffusion, and R_{ct} and CPE2 are related to charge transfer. The charge transfer resistance, R_{ct}, is inversely proportional to the rate of the corresponding hydrogen adsorption reaction. For the kinetically controlled HER, the R_{ct} value could be used as the basis to study the activity trend of electrocatalyst.

Table. S1 Comparison of HER performance with previously reported phosphide-metal oxide nanostructured electrocatalysts under alkaline condition.

catalyst	η_{10} (mV)	η_{100} (mV)	Reference
Ni_2P-NiMoOx nanocones	**49**	**137**	**This work**
Crystalline Ni_2P-Amorphous $NiMoO_x$	91	188	[1]
NiP_2@MoO_2/Co(Ni)MoO_4	66 (η_{50})	131	[2]
FeCo/Co_2P@NPCF	260	380	[3]
V-Ni_2P/$Ni_{12}P_5$	62	146	[4]
V-CoP@a-CeO_2	68	140	[5]
O-CoP	98	150	[6]
MnO_x/NiFeP	-	214	[7]
NiMnOP	91	145	[8]
MoO_2/Mo_3P/Mo_2C	69	155	[9]

Table. S2 the fitting values of different catalyst equivalent circuits

Catalyst	**R_s (Ω)**	**R_w (Ω)**	**R_{ct} Ω)**
Ni-BDC	1.275	1.646	24.510
$NiMoO_x$	1.291	0.500	19.330
Ni_2P	1.235	0.055	6.203
$Ni_2P/NiMoO_x$	1.365	0.097	1.460

Table. S3 The fitting values of the equivalent circuits of $Ni_2P/NiMoO_x$ catalysts

Catalyst	R_s (Ω)	R_w (Ω)	R_{ct} (Ω)
$Ni_2P/NiMoO_x$ nanocones	1.365	0.097	1.460
$Ni_2P/NiMoO_x$ nanorods	1.270	0.677	2.981

Model	Nanocone	Nanorod	Nanocuboid (3 times length)
Tip surface charge density (C m^{-2})	-0.11	-0.09	-0.06

Table. S4 Calculation results from COMSOL

References

[1] J.T. Ren, L. Chen, H.Y. Wang, W.W. Tian, X.L. Song, Q.H. Kong, Z.Y. Yuan, Synergistic Activation of Crystalline Ni2P and Amorphous NiMoOx for Efficient Water Splitting at High Current Densities[J]. *ACS Catalysis,* 2023, 13, 9792-9805. https://doi.org/10.1021/acscatal.3c01885.

[2] Q. Xu, P. Wang, L. Wan, Z. Xu, M. Z. Sultana, B. Wang, Superhydrophilic/Superaerophobic Hierarchical NiP_2@MoO_2/Co(*Ni*)MoO_4 Core–Shell Array Electrocatalysts for Efficient Hydrogen Production at Large Current Densities[J]. *ACS Applied Materials & Interfaces,* 2022, 14, 19448-19458. https://doi.org/10.1021/acsami.2c01808.

[3] Q. Shi, Q. Liu, Y. Ma, Z. Fang, Z. Liang, G. Shao, B. Tang, W. Yang, L. Qin, X. Fang, High-Performance Trifunctional Electrocatalysts Based on FeCo/Co_2P Hybrid Nanoparticles for Zinc–Air Battery and Self-Powered Overall Water Splitting[J]. *Adv. Energy Mater.,* 2020, *10*, 1903854. https://doi.org/10.1002/aenm.201903854.

[4] T. Zhao, S. Wang, Y. Li, C. Jia, Z. Su, D. Hao, B. J. Ni, Q. Zhang, C. Zhao, Heterostructured V-Doped Ni_2P/$Ni_{12}P_5$ Electrocatalysts for Hydrogen Evolution in Anion Exchange Membrane Water Electrolyzers[J]. *Small,* 2022, *18*, 2204758. https://doi.org/10.1002/smll.202204758.

[5] L. Yang, R. Liu, L. Jiao, Electronic Redistribution: Construction and Modulation of Interface Engineering on CoP for Enhancing Overall Water Splitting[J]. *Adv. Funct. Mater.,* 2020, *30*, 1909618. https://doi.org/10.1002/adfm.201909618.

[6] G. Zhou, M. Li, Y. Li, H. Dong, D. Sun, X. Liu, L. Xu, Z. Tian, Y. Tang, Regulating the Electronic Structure of CoP Nanosheets by O Incorporation for High-Efficiency Electrochemical Overall Water Splitting[J]. Adv. Funct. Mater., 2020, 30, 1905252. https://doi.org/10.1002/adfm.201905252.

[7] P. Wang, Y. Luo, G. Zhang, M. Wu, Z. Chen, S. Sun, Z. Shi, MnOx-Decorated Nickel-Iron Phosphides Nanosheets: Interface Modifications for Robust Overall Water Splitting at Ultra-High Current Densities[J]. *Small,* 2022, *18*, 2105803. https://doi.org/10.1002/smll.202105803.

[8] J. Balamurugan, T. T. Nguyen, V. Aravindan, N. H. Kim, J. H. Lee, Highly reversible water splitting cell building from hierarchical 3D nickel manganese oxyphosphide nanosheets[J]. *Nano Energy,* 2020, *69*, 104432. https://doi.org/10.1016/j.nanoen.2019.104432.

[9] J. Xiao, S. Zhang, Y. Sun, X. Liu, G. He, H. Liu, J. Khan, Y. Zhu, Y. Su, S. Wang, L. Han, Urchin-Like Structured MoO2/Mo3P/Mo2C Triple-Interface Heterojunction Encapsulated within Nitrogen-Doped Carbon for Enhanced Hydrogen Evolution Reaction[J]. *Small*, 2023, 19, 2206472. https://doi.org/10.1002/smll.202206472.